Acta Crystallographica Section D
Biological Crystallography
ISSN 0907-4449

Structural studies show that the A178L mutation in the C-terminal hinge of the catalytic loop-6 of triosephosphate isomerase (TIM) induces a closed-like conformation in dimeric and monomeric TIM

Markus Alahuhta,[a]‡ Marco G. Casteleijn,[b]‡ Peter Neubauer[b] and Rik K. Wierenga[a]*

[a]Biocenter Oulu and Department of Biochemistry, University of Oulu, PO Box 3000, FIN-90014 University of Oulu, Finland, and [b]Biocenter Oulu and Bioprocess Engineering Laboratory, Department of Process and Environmental Engineering, University of Oulu, Finland

‡ These authors contributed equally to this work.

Correspondence e-mail: rik.wierenga@oulu.fi

Received 18 October 2007
Accepted 14 November 2007

PDB References: A178L, unliganded, 2v0t, r2v0tsf; A178L, liganded, 2v2c, r2v2csf; ml1A178L, unliganded, 2v2d, r2v2dsf; ml1A178L, liganded, 2v2h, r2v2hsf.

The flexible catalytic loop, loop-6, of TIM has evolved to preferably be open in the unliganded state and to preferably be closed in the liganded state. The N-terminal and C-terminal hinges of this loop are important for its opening/closing mechanism. In this study, a small conserved C-terminal hinge residue, Ala178, has been mutated into a residue with a larger side chain, Leu178. This mutation has been made in the dimeric trypanosomal wild-type TIM (wtTIM) and in its mutated catalytically competent monomeric variant (ml1TIM). The variants are referred to as A178L and ml1A178L, respectively. Crystal structures have been determined of unliganded A178L (at 2.2 Å), liganded A178L (at 1.89 Å), unliganded ml1A178L (at 2.3 Å) and liganded ml1A178L (at 1.18 Å) using the transition-state analogue 2-phosphoglycolate as a ligand. Structural characterization of the two variants shows that this mutation favours the closed conformation of the C-terminal hinge region, even in the absence of ligand. In the structure of the unliganded A178L variant a range of new loop-6 conformations are observed, including subunits in which the tip of loop-6 is completely disordered. The catalytic efficiency of A178L is lower than that of wtTIM, which correlates with the structural differences between the apo forms of wtTIM and A178L, in particular the more disordered loop-6 in the structure of unliganded A178L. In the liganded structures of A178L and ml1A178L the structural differences induced by the mutation are minimal. Structural characterization of the ml1A178L variant highlights its structural plasticity.

1. Introduction

Flexible loops are known to play key roles in many reaction mechanisms. In triosephosphate isomerase (EC 5.3.1.1; TIM) this involves loop-6, residues Pro168–Ala178, which immediately follows the catalytic residue Glu167 (Joseph *et al.*, 1990; Sun & Sampson, 1999). Wild-type TIM (wtTIM) is a homodimeric enzyme that catalyses the isomerization of D-glyceraldehyde-3-phosphate (D-GAP) and dihydroxyacetone phosphate (DHAP; Fig. 1; Knowles, 1991). This is an important reaction of the glycolytic pathway; TIM deficiency owing to mutations in the TIM gene causes severe neurological diseases (Gnerer *et al.*, 2006; Orosz *et al.*, 2006; Ralser *et al.*, 2006).

The structural, energetic and dynamical properties of the flexible catalytic loop-6 of TIM have been studied extensively using various experimental and theoretical approaches (Berlow *et al.*, 2007; Desamero *et al.*, 2003; Eaazhisai *et al.*, 2004; Kempf *et al.*, 2007; Massi *et al.*, 2006; Nickbarg & Knowles, 1988; Pattanaik *et al.*, 2003; Williams & McDermott, 1995). In the presence of substrate the loop is preferably

closed, whereas in the absence of substrate the loop is preferably open. Elegant NMR studies have shown that in the liganded (closed) and the unliganded (open) states loop-6 still alternates between the closed and open conformations and it has been found that this occurs with a frequency which is optimally complementary to the timing of the catalytic cycle (Rozovsky *et al.*, 2001; Rozovsky & McDermott, 2001). In its closed conformation, loop-6 is hydrogen bonded to loop-7 and to the phosphate moiety of the substrate. In this conformation it seals off the catalytic cavity from bulk solvent, stabilizes the mode of binding of the substrate and enables the catalytic glutamate to adopt its correct 'swung-in' position for catalysis (Lolis & Petsko, 1990; Sampson & Knowles, 1992*a*,*b*; Wierenga, Noble, Vriend *et al.*, 1991). The proton-transfer steps of the catalytic mechanism have also been studied by NMR (Amyes & Richard, 2007; Harris *et al.*, 1997).

Protein crystallographic studies have shown that the closing of loop-6 is correlated with a structural change in the neighbouring loop, loop-7, which has the characteristic Tyr210-Gly211-Gly212-Ser213 sequence (Casteleijn *et al.*, 2006; Kursula *et al.*, 2004). The tip of loop-6 moves by about 7 Å, whereas the structural change of loop-7 involves rotations of the peptide planes between Gly211-Gly212 and Gly212-Ser213. Correlated with the structural changes of loop-6 and loop-7 is a movement of the side chain of the catalytic glutamate from the 'swung-out' conformation (pointing away from the substrate) to the catalytically competent 'swung-in' conformation (pointing towards the substrate). Detailed structural studies have shown that the five residues (Ala171-Ile172-Gly173-Thr174-Gly175) of the tip of loop-6 move as a rigid body (Joseph *et al.*, 1990; Wierenga, Noble, Postma *et al.*, 1991). The importance of the tip of this loop for the function of TIM has been confirmed by studying the properties of a variant of chicken TIM in which these residues were deleted (Pompliano *et al.*, 1990). The movement of the tip residues is achieved by relatively small changes in the φ/ψ values of the residues in the N-terminal and C-terminal hinge tripeptides. The N-terminal hinge occurs immediately after the catalytic residue Glu167 and the N-terminal hinge sequence (residues Pro168-Val169-Trp170) is highly conserved (Kursula *et al.*, 2004; Sun & Sampson, 1999; Xiang *et al.*, 2004). The C-terminal hinge tripeptide, residues Lys176-Val177-Ala178 in trypanosomal TIM, is not fully conserved but certain sequence preferences have been observed. The importance of the conserved sequence patterns of the C-terminal hinge have also been confirmed by elegant directed-evolution experiments followed up by enzymological and protein crystallographic studies (Kursula *et al.*, 2004; Sun & Sampson, 1999; Xiang *et al.*, 2004). For example, the variant of chicken TIM in which the C-terminal hinge tripeptide was changed from KTA to YSL was characterized very extensively. Protein crystallographic studies of this triple-mutant variant of chicken TIM showed that the side chain of Ala178 points inwards into a hydrophobic pocket shaped by the side chains of Pro168, Trp170, Ala183, Tyr210 and Leu222. A bulky residue at this site clashes, particularly with the Trp170 side chain of loop-6, when this loop is in the open conformation. In the closed conformation, the Ala178 and Trp170 side chains move away from each other (Fig. 2) and a more bulky residue at position 178 is possible (Kursula *et al.*, 2004). In this closed confor-

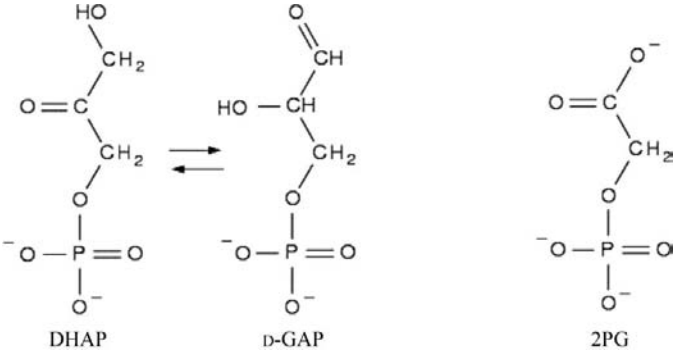

Figure 1
The reaction scheme of TIM and the covalent structure of the transition-state analogue 2-phosphoglycolate (2PG).

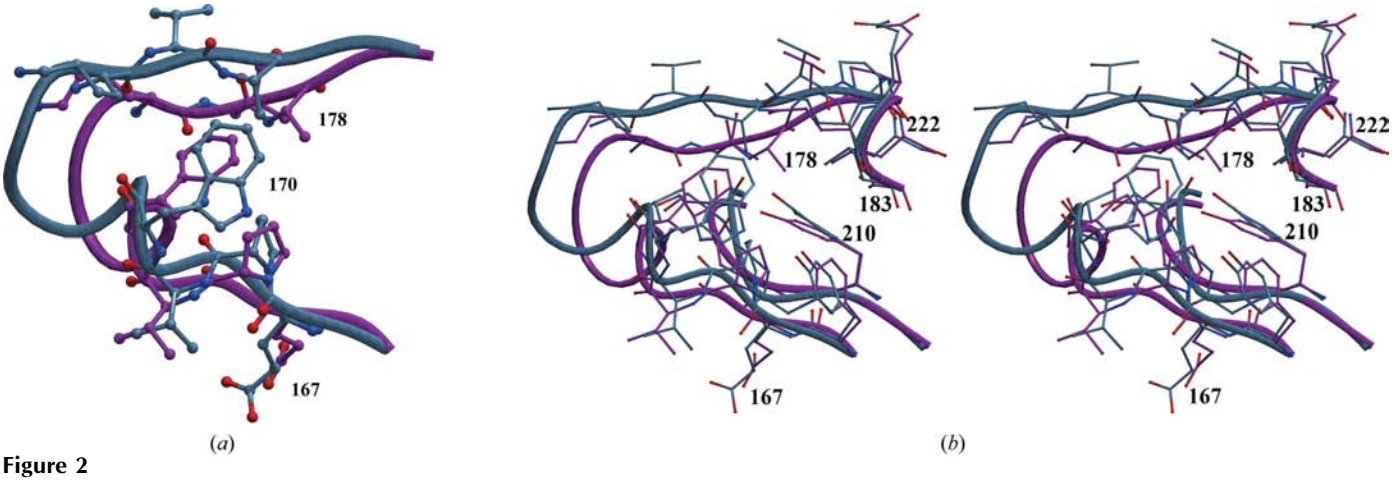

Figure 2
Comparison of the open (unliganded, 5tim, cyan) and closed (liganded, 1n55, magenta) structures of wild-type TIM (top view). (*a*) The open structure of loop-6 is coloured cyan; the closed structure is coloured magenta. (*b*) Stereo picture, showing the environment of Ala178 in the open (cyan) and closed (magenta) conformation.

mation, Ala178 moves near to the side chain of Tyr210 of loop-7, which adopts a somewhat bent conformation (Fig. 2) and Tyr210 OH becomes hydrogen bonded to Gly212 O of loop-7 and to Ala178 N of loop-6 (Berlow *et al.*, 2007; Kursula *et al.*, 2004).

Sequence analyses of 133 sequences have shown that two families of loop-6 sequences can be recognized (Kursula *et al.*, 2004): one family contains the sequences from eubacteria and eukaryotes (114 sequences) and the other the sequences from archaebacteria (19 sequences). These two sequence families are clearly different and therefore the sequence-conservation patterns important for the studies reported here are taken from the 114 eubacterial and eukaryotic sequences. Neither aromatic residues nor glycines are observed in the sequences of the C-terminal hinge tripeptide. The first residue of the N-terminal hinge is always a proline (Kursula *et al.*, 2004) and structural enzymological studies have indicated that this proline is important for the concerted movement of loop-6 and loop-7 (Casteleijn *et al.*, 2006). Recent NMR studies of a variant in which the sequence of the N-terminal hinge was changed to Pro-Gly-Gly and that of the C-terminal hinge was changed to Gly-Gly-Gly have shown that the dynamical properties of this mutated loop-6 have changed, resulting in a 1000-fold lower turnover number and a tenfold higher K_m (Kempf *et al.*, 2007). The residue observed at the last position of the C-terminal hinge (Ala178 in wild-type trypanosomal TIM) is an alanine in 94 sequences (out of 114); a proline (seven out of 114), a serine (ten out of 114) or a cysteine (three out of 114) are also observed with lower frequencies (Kursula *et al.*, 2004). A bulky residue is never observed at this position. This position is at the back side of the molecule (this is best visualized in Fig. 8) and the distance between the C^{α} of Ala178 and the catalytic base (Glu167 OE2) is 11 Å in the closed liganded conformation.

The characterization of the YSL triple-mutant variant of chicken TIM suggested that the bulky side chain of leucine favours the closed loop-6 conformation. In wtTIM, the permanently closed loop-6 will interfere with efficient binding since in the closed form access to the catalytic site is blocked, but in the monomeric variant the solvent-accessibility of the catalytic site is much higher owing to the absence of the second subunit. In order to test this hypothesis, the effect of the point mutation A178L on the structural and enzymological properties of the dimeric wild-type trypanosomal TIM (postulated to have lower catalytic efficiency) and its monomeric variant ml1TIM (postulated to have higher catalytic efficiency) have been determined.

ml1TIM was generated from wtTIM by deleting loop-3 (the dimer-interface loop; Borchert *et al.*, 1993). In addition, the sequence of loop-1 was changed and shortened by one residue and in loop-4 an alanine (Ala100) was mutated to a tryptophan (Schliebs *et al.*, 1996; Thanki *et al.*, 1997). The latter mutation stabilizes the active conformation of loop-4, but has very little effect on its kinetic properties (Borchert *et al.*, 1995; Schliebs *et al.*, 1996). The structural and enzymological properties of ml1TIM have been extensively characterized (Thanki *et al.*, 1997) and it has been found that the k_{cat} value of the monomeric form is approximately 1000-fold lower when compared with the wild type, whereas the K_m value is increased tenfold, indicating significantly lower affinity. These kinetic differences correlate with a much more solvent-accessible catalytic site; the catalytic loops also have increased conformational flexibility (Borchert *et al.*, 1995). ml1TIM is a competent catalyst, but the details of the reaction mechanism and the rate-limiting steps of ml1TIM and wild-type dimeric TIM may differ. In any case, as is shown in Fig. 3, the mode of binding of the transition-state analogue 2-phosphoglycolate (2PG) to wild-type TIM and monomeric ml1TIM is different. In the atomic resolution structure of the wild-type TIM–2PG complex, two modes of binding are observed: a major and a minor conformation (Kursula & Wierenga, 2003). Fig. 3 illustrates that the principal mode of binding of this transition-state analogue to ml1TIM is the same as observed for the minor mode of binding in wild-type TIM. Monomeric TIMs are also less stable than wild-type TIM.

The crystal structures of unliganded/liganded A178L and unliganded/liganded ml1A178L are described using the transition-state analogue 2-phosphoglycolate as a ligand

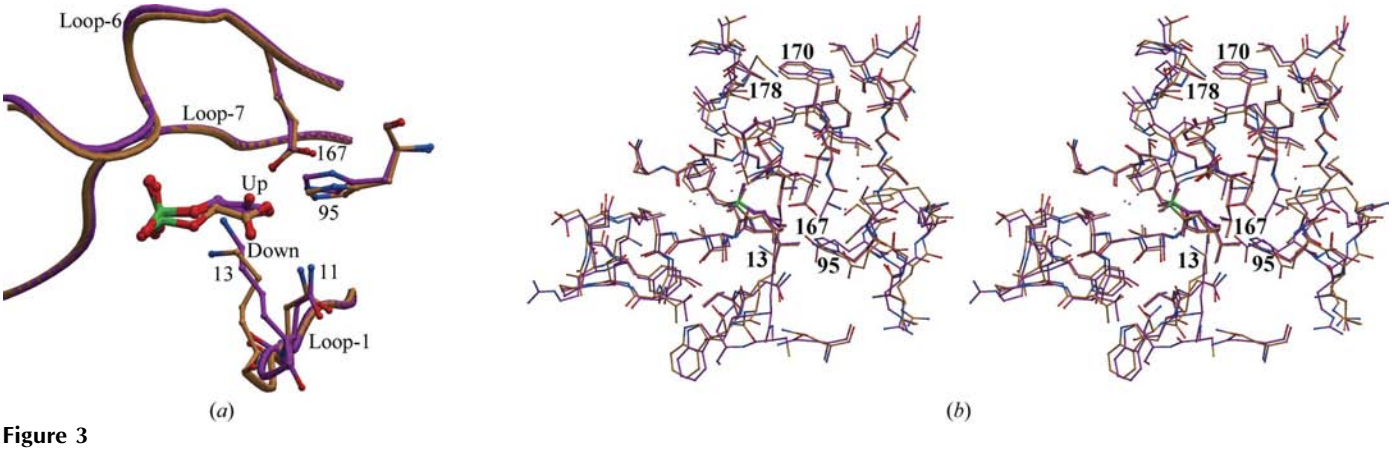

Figure 3
Comparison of the structures of liganded wtTIM (1n55) and liganded ml1TIM (1ml1). (*a*) Schematic view. (*b*) Stereo picture. The wtTIM structure is coloured magenta and the ml1TIM structure is coloured gold. In wtTIM the carboxyl moiety of the ligand has a double conformation (up and down). The up conformation is the major conformation. In the structure of the ml1TIM–2PG complex only the down conformation is observed.

Table 1
Overview of structures and crystallization conditions.

	A178L	A178L–2PG	ml1A178L	ml1A178L–2PG
Well solution	0.1 *M* HEPES pH 7.5, 8% ethylene glycol, 10% PEG 8000	0.1 *M* TEA pH 7.5, 2% PEG 400, 2.0 *M* $(NH_4)_2SO_4$	1.75 *M* $(NH_4)_3PO_4$ pH 8.2	0.1 *M* citrate pH 5.5, 20% PEG 6000, 3% *t*-butanol
Crystallization temperature (K)	295	295	295	295
Cryosolution	None	25% ethylene glycol in well solution	15% ethylene glycol in well solution	20% ethylene glycol in well solution
Space group	$P2_1$	$P2_12_12$	$P6_3$	$C2$
V_M (Å^3 Da^{-1})	2.6	3.3	2.6	2.2
No. of subunits per ASU	8	1	1	3
Resolution (Å)	2.2	1.89	2.3	1.18
PDB code	2v0t	2v2c	2v2d	2v2h

(Fig. 1). Complementary enzymological studies show that these A178L variants have a lower catalytic efficiency, which is discussed in the context of the refined structures.

2. Materials and methods

2.1. Materials, mutagenesis, protein expression and protein purification

Unless specifically mentioned, all commercial chemicals were used without further purification as described previously (Casteleijn *et al.*, 2006). Site-directed mutagenesis was performed by PCR using the QuikChange site-directed mutagenesis kit (Stratagene). The expression plasmid pET3a (Novagen) containing the genes for wtTIM or ml1TIM was used as a template. The following mutagenic primers were used: A178L sense (+), 5′-CATTGGTACCGGCAAGGTG-CTGACACCACAGC-3′, and A178L compl. (−), 5′-GCTG-TGGTGTCAGCACCTTGCCGGTACCAATG-3′.

The complete DNA sequences of the new genes including the mutations were verified by sequencing with the DYEnamic ET terminator cycle sequence kit (GE Healthcare). *Escherichia coli* TOP10 cells (Invitrogen) were used as the host strain for plasmid production. Plasmids were then transformed into *E. coli* BL21 pLysS (Invitrogen) for protein production. The protein-expression and purification protocols were similar to those described previously (Casteleijn *et al.*, 2006). Protein concentrations were determined by OD_{280} with a nanodrop spectrophotometer (Nanodrop) and correlated using a Bradford and Micro BSA kit (Pierce). The reference molar extinction coefficients of 35 075 M^{-1} cm^{-1} (dimeric TIMs) and 40 575 M^{-1} cm^{-1} (monomeric TIMs) were calculated using the *ProtParam* tool (Gasteiger *et al.*, 2003). The purified protein was stored in 20 m*M* Tris–HCl, 100 m*M* NaCl pH 7.0 (at 298 K) at 203 K after quick freezing in liquid nitrogen.

2.2. Enzymatic assays

The triosephosphate isomerase activity of wtTIM and ml1TIM was assayed at 298 K as described previously (Sun & Sampson, 1999). With D-GAP as substrate, the assay mixture contained 0.3 m*M* NADH, 0.04 mg ml^{-1} glycerolphosphate dehydrogenase (GDH) and 0.1–9 m*M* D-GAP in 0.3 ml buffer [100 m*M* triethanolamine (TEA), 1 m*M* ethylenediamine tetraacetic acid (EDTA), 1 m*M* reduced dithiothreitol (DTT), 1 m*M* NaN_3 pH 7.6 (at 298 K)]. Residual TIM activity in the GDH sample was inactivated by incubation with bromohydroxyacetone phosphate as described previously (Sun & Sampson, 1999). 4.5 ng wtTIM, 3.3 ng A178L, 1.6 µg ml1TIM or 63 µg ml1A178L was used to initiate the reaction. With DHAP as substrate, the assay mixture contained 0.3 m*M* NAD^+, 5 m*M* potassium arsenate, 0.17 mg ml^{-1} glyceraldehyde-3-phosphate dehydrogenase and 0.3–40 m*M* DHAP. 98 ng wtTIM, 80 ng A178L, 12 µg ml1TIM or 50 µg ml1A178L was used to initiate the reaction. Initial rates were measured at each substrate concentration from the change in NADH absorbance at 340 nm using a Powerwave X microtitre plate reader (Bio-tek Instruments). Path-length corrections were measured according to the manufacturer and were confirmed with 0.05 m*M* NADH solution using a spectrophotometer and a 1 cm cuvette at 340 nm. The k_{cat} and K_m values were obtained after data fitting to the Michaelis–Menten equation using *GraFit* (Erithacus Software, Staines, England). K_i values for arsenate and 2PG were determined assuming a competitive inhibition model (Sun & Sampson, 1999).

2.3. Thermal stability

Circular-dichroism (CD) spectra were recorded using a Jasco J-715 spectropolarimeter with a path length of 1 mm at 298 K before and after the temperature-induced denaturation studies. A baseline spectrum of the buffer was subtracted from the sample spectra. Temperature-induced denaturation studies were carried out by monitoring the ellipticity at 222 nm from 293 to 333 K with a rate of 30 K h^{-1}. Samples were kept at 333 K for less than 1 min, after which the ellipticity was monitored from 333 to 293 K. Protein solutions (0.3 mg ml^{-1}) were either in 0.9 m*M* TEA, 1.2 m*M* NaCl pH 7.5 (unliganded enzyme) or in 2 m*M* 2PG, 0.9 m*M* TEA, 1.2 m*M* NaCl pH 7.5 (enzyme liganded with 2PG). The protein solutions also contained 0.05 m*M* DTT, 0.05 m*M* EDTA and 0.05 m*M* sodium azide and were degassed before the measurements.

2.4. Crystallography

Crystallization conditions were initially screened using the Factorial 1 screen (Zeelen *et al.*, 1994) at 295 K with the hanging-drop method. The drops were made by mixing 2 µl

Table 2
Data-processing and refinement statistics.

Values in parentheses are for the highest resolution bin.

	A178L	A178L–2PG	ml1A178L	ml1A178L–2PG
Data collection				
Beamline	Home source	Home source	BW7B	BW7A
Wavelength (Å)	1.5418	1.5418	0.847	0.793
Detector	MAR 345	MAR 345	MAR 345	CCD 165
Temperature (K)	100	100	100	100
Space group	$P2_1$	$P2_12_12$	$P6_3$	$C2$
Unit-cell parameters				
a (Å)	76.69	119.23	95.23	68.26
b (Å)	79.25	59.29	95.23	117.99
c (Å)	174.00	46.95	48.82	81.77
α (°)	90.00	90.00	90.00	90.00
β (°)	99.22	90.00	90.00	95.84
γ (°)	90.00	90.00	120.00	90.00
Resolution range (Å)	25–2.2 (2.3–2.2)	25–1.89 (1.95–1.89)	25–2.3 (2.35–2.3)	25–1.18 (1.4–1.18)
$R_{\rm merge}$ (%)	11.0 (39.9)	2.7 (6.4)	8.1 (22.5)	5.6 (34.7)
$I/\sigma(I)$	13.4 (3.4)	63.3 (27.0)	24.5 (13.3)	17.8 (1.0)
Completeness (%)	98.4 (88.3)	99.5 (95.5)	99.2 (99.9)	99.9 (100)
Redundancy	4.5 (3.3)	8.5 (6.1)	12.1 (12.4)	5.2 (5.2)
No. of unique reflections	103058	27265	11321	210261
Wilson B factor (Å^2)	28.3	18.5	39.1	14.0
Refinement				
Resolution range (Å)	25–2.2	20–1.89	25–2.3	25–1.18
Protein atoms	14895	1842	1836	5514
Ligand atoms	80	24	5	30
Water molecules	1471	527	133	842
R (%)	17.8	13.9	20.1	13.9
$R_{\rm free}$ (%)	23.9	18.2	27.0	18.7
R.m.s.d. bond length (Å)	0.014	0.022	0.015	0.014
R.m.s.d. bond angle (°)	1.5	1.7	1.5	
R.m.s.d. bond angle (DANG) (Å)				0.030
Anisotropic displacement parameters				
DELU (Å^2)				0.050
SIMU (Å^2)				0.053
ISOR (Å^2)				0.097
R.m.s.d. B factors (Å^2)				
Main chain	0.6	0.6	0.6	1.2
Side chain	1.7	2.0	1.6	3.2
Average B (Å^2)				
Protein	13.6	10.3	15.1	13.1
2PG		15.1		7.4
Ramachandran plot (Lovell *et al.*, 2003)				
Allowed region (%)	99.9	100.0	99.6	99.7
No. of outliers†	2	0	1	2

† The outliers have been checked and found to be close to allowed regions or to have high B factors.

protein solution and 2 µl well solution. The protein solution used for all crystallization experiments was 11 mg ml^{-1} protein, 20 m*M* Tris–HCl pH 7, 100 m*M* NaCl, 1 m*M* DTT, 1 m*M* EDTA and 1 m*M* NaN_3. In the case of A178L, 0.2 m*M* Triton X-100 was also added to the protein solution. The liganded crystals were grown by adding 10 m*M* 2PG to the protein solution. Whenever necessary, further optimization was performed to increase crystal quality. The well solutions used in the crystallization experiments that led to the four structures are presented in Table 1. Essential data-collection and refinement parameters of these structures are shown in Table 2.

The data sets collected at the home source were obtained using a Nonius FR591 rotating-anode X-ray generator equipped with a MAR Research MAR345 image plate. The synchrotron data sets were collected at EMBL/DESY, Hamburg, Germany on beamline BW7A using a MAR Research MAR CCD 165 mm detector and on beamline BW7B using a MAR Research MAR345 image plate. The crystals of A178L–2PG, unliganded ml1A178L and ml1A178L–2PG were briefly transferred into a cryosolution (Table 1). Prior to picking up a crystal out of the crystallization/cryosolution drop, 2 µl 50%(*v*/*v*) paraffin oil in silicone oil was added on top of the crystallization drop to prevent the crystals from drying out. Harvested crystals were flash-frozen in a cold nitrogen stream at 100 K before data collection. All data were processed using the program *XDS* (version December 2003; Kabsch, 1993) with the *XDSi* v.1.2 interface (Kursula, 2004). The programs *F2MTZ* and *CAD* from the *CCP*4 package (v.6.02; Collaborative Computational Project, Number 4, 1994) were used to flag 5% of the observed structure factors for free *R*-factor calculations. The structures were solved using molecular replacement with the program *MOLREP* v.7.3.01 (Vagin & Teplyakov, 1997) using wild-type trypanosomal TIM (PDB code 5tim; Wierenga, Noble, Vriend *et al.*, 1991) as a search model for the wtTIM structures and engineered monomeric TIM (PDB entry 1ml1; Thanki *et al.*, 1997) for the monomeric variants. In each of the structure determinations, the loop-6 residues were deleted from the search model and rebuilt in the new electron-density maps. Waters, 2PG and other solvent molecules were also built from scratch in the respective electron-density maps. Three structures were refined with *REFMAC*5 v.5.3.0022 (Murshudov *et al.*, 1997). NCS restraints were used in the *REFMAC*5 refinement protocol for the unliganded A178L structure. The anisotropic motion of the subunits was described using TLS parameters as implemented in *REFMAC*5 (Murshudov *et al.*, 1997) for the unliganded A178L and ml1A178L structures. The atomic resolution structure of ml1A178L–2PG was refined using *SHELXH* v.97-2 (Sheldrick & Schneider, 1997). The program *Coot* v.0.2 (Emsley & Cowtan, 2004) was used for the manual rebuilding of the structures, for the addition of waters and for checking the quality of the structures. The *MOLPROBITY* method (Lovell *et al.*, 2003) was used to analyze the Ramachandran plot.

2.5. Structure analysis

For the structure comparisons, the following structures were used: trypanosomal TIM refined at 1.83 Å (PDB code 5tim; Wierenga, Noble, Vriend *et al.*, 1991), *Leishmania mexicana* TIM complexed with 2PG refined at 0.83 Å (PDB code 1n55; Kursula & Wierenga, 2003), trypanosomal TIM complexed with sulfate refined at 2.4 Å (PDB code 2v5l; Noble *et al.*, 1993), ml1TIM complexed with 2PG refined at 2.6 Å (PDB code 1ml1; Thanki *et al.*, 1997), *Plasmodium falciparum* TIM complexed with 2PG, 2.8 Å resolution (PDB code 1lzo; Parthasarathy *et al.*, 2002), unliganded YSL chicken TIM, 2.9 Å resolution (PDB code 1ssd; Kursula *et al.*, 2004) and YSL chicken TIM complexed with 2PG, 2.9 Å resolution (PDB code 1ssg; Kursula *et al.*, 2004). In 5tim, the *A* subunit is unliganded (open). In the atomic resolution structure of 1n55 there is only one subunit per asymmetric unit and this structure is used as the reference structure for the wtTIM liganded (closed) complex, as the *L. mexicana* TIM and trypanosomal TIM are very closely related (Williams *et al.*, 1999). In this manuscript, we use the trypanosomal TIM numbering scheme, in which the catalytic glutamate is Glu167 and loop-6 has the following sequence: Pro168-Val169-Trp170-Ala171-Ile172-Gly173-Thr174-Gly175-Lys176-Val177-Ala178. The superpositions of the various structures on each other were performed using the 36 C^{α} atoms of the β-sheet residues numbered 7–11, 38–42, 61–64, 90–93, 122–127, 163–166, 207–210 and 230–233. The structures were analyzed with the programs *O* (Jones *et al.*, 1991), *Coot* v.0.2 (Emsley & Cowtan, 2004) and *ICM* v.3.5-1 (Molsoft LLC, La Jolla, USA; http://www.molsoft.com).

The program *Chemtool* (http://ruby.chemie.uni-freiburg.de/~martin/chemtool/) was used to generate Fig. 1. *ICM* was used to produce Figs. 2, 3 and 5–9. The program *GIMP* (http://www.gimp.org) was used to edit and label Figs. 1–3 and 5–9.

3. Results and discussion

3.1. Enzyme kinetics and thermal stability

The kinetic data are summarized in Table 3. For wild-type TIM it is seen that the A178L mutation causes little change in k_{cat}, but gives rise to somewhat higher K_m values. For the ml1A178L variant, tenfold lower k_{cat} and similar K_m values are observed compared with ml1TIM. For both variants the affinity for the transition-state analogue 2PG is lower (Table 3). The CD melting curves (Fig. 4) show that the stability of the unliganded forms of the variants is affected much more than the stability of the liganded forms. This is particularly prominent for the ml1A178L variant. The unfolding curve of the unliganded form shows partial unfolding even at 298 K, being approximately 25% unfolded at 308 K. For each of the variants it is found that heat-induced denaturation is irreversible, as deduced from refolding experiments when cooling the sample back to 293 K after

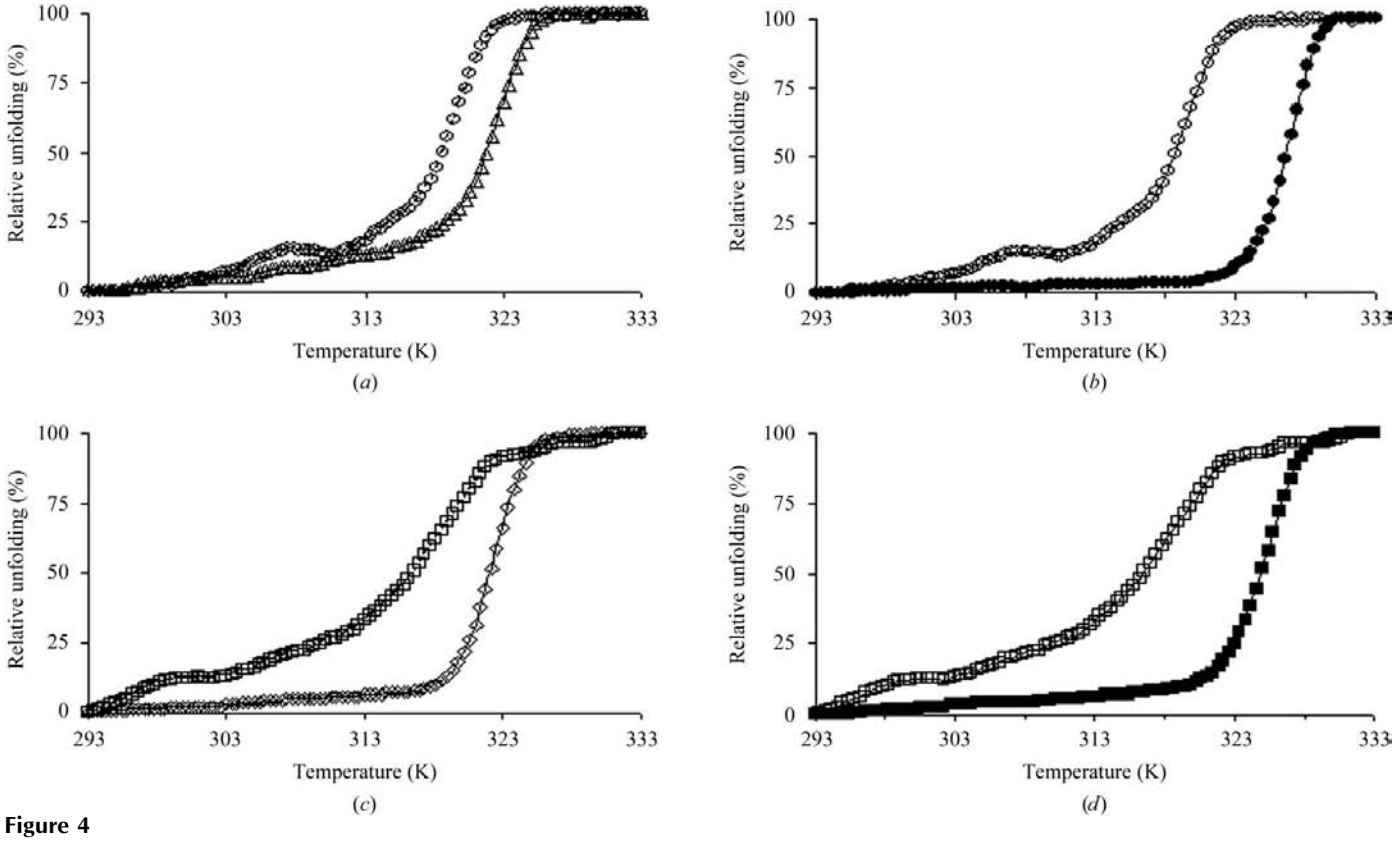

Figure 4
CD melting curves. (*a*) wtTIM (triangles) and A178L (circles). (*b*) A178L (circles) and A178L in the presence of 2PG (filled circles). (*c*) ml1TIM (diamonds) and ml1A178L (squares). (*d*) ml1A178L (squares) and ml1A178L in the presence of 2PG (filled squares).

Table 3
Kinetic data for the two variants.

	D-GAP			DHAP			AsO_4^{3-}	2PG
	K_m (m*M*)	k_{cat} (s^{-1})	k_{cat}/K_m (mM^{-1} s^{-1})	K_m† (m*M*)	k_{cat}† (s^{-1})	k_{cat}/K_m (mM^{-1} s^{-1})	K_i (m*M*)	K_i (m*M*)
wtTIM‡	0.26 ± 0.04	4400 ± 530	16800 ± 3400	0.9 ± 0.3	800 ± 140	900 ± 270	4.9 ± 0.1	0.05§
A178L	0.61 ± 0.07	5300 ± 500	8700 ± 1200	1.4 ± 0.8	500 ± 240	350 ± 280	7.8 ± 2.5	0.39 ± 0.14
ml1TIM	3.8 ± 1.9	2.2 ± 1.0	0.58 ± 0.40	7.6 ± 2.9	0.8 ± 0.3	0.11 ± 0.06	5.1 ± 0.5	ND¶
ml1A178L	3.3 ± 1.1	0.25 ± 0.18	0.08 ± 0.06	9.3 ± 4.6	0.06 ± 0.02	0.006 ± 0.004	17.9 ± 2.0	0.17 ± 0.06

† Measured in the presence of 5 m*M* AsO_4^{3-}. ‡ wtTIM data as previously published (Casteleijn *et al.*, 2006). § All values except K_i (2PG) of wtTIM are the average of multiple independent measurements. ¶ ND, not determined. The literature value is 0.045 m*M* (Thanki *et al.*, 1997).

completion of the heat-induced denaturation protocol (data not shown).

3.2. Structural studies of the A178L variant

Crystal structures have been determined for the unliganded and liganded forms of the A178L variant of wild-type trypanosomal TIM (Table 1). The unliganded A178L was crystallized in a crystal form with eight subunits (four dimers) per asymmetric unit, whereas in the liganded A178L crystal form there is only one subunit per asymmetric unit. These two structures were refined with *REFMAC*5 (Murshudov *et al.*, 1997) and final models with good geometry and *R* factors were obtained (Table 2). In the unliganded structure a bound sulfate ion is observed in the vicinity of each of the active sites. This sulfate is most likely to be present as an impurity in the 4-(2-hydroxyethyl)-1-piperazine-ethanesulfonic acid (HEPES) buffer used in the well solution of the crystallization setup. This sulfate ion is bound 1.5 Å further away from the catalytic site compared with the classical phosphate-binding site. Such a mode of binding has been described before as the binding site for a sulfate ion to the open conformation of loop-7 of trypanosomal TIM (PDB code 2v5l; Noble *et al.*, 1993) and for the mode of binding of the phosphate moiety of 2PG when bound to the open conformation of the active site of *P. falciparum* TIM (PDB code 1lzo; Parthasarathy *et al.*, 2002). After superposition, the corresponding S and P atoms of the three complexes are within 0.4 Å of each other.

Comparison of the loop-6 conformation in each of the eight unliganded subunits of the asymmetric unit shows a large structural variability that has not been observed in any of the many unliganded structures deposited in the PDB. The structural differences of these eight subunits from wtTIM coincide with the loop-6 region, Glu167–Leu178. Small concerted shifts (approximately 1 Å) are also seen for the helical region of loop-5, residues 128–138, but no other structural changes are seen. The loop-5 region, in particular the side chain of the conserved Glu129, is hydrogen bonded to loop-6 in wild-type TIM and is also slightly rearranged in wild-type TIM when ligand binding induces the closed conformation. In each of the eight subunits of unliganded A178L the side chain of the catalytic glutamate Glu167 adopts the same conformation as in unliganded wild type, being in the 'swung-out' conformation, and the neighbouring loop-7 is also in the open unliganded conformation as in the wild type.

In each of the eight independent structures the Leu178 side chain is well defined and it is seen that the C-terminal hinge region has adopted a non-wild-type conformation in each subunit. In seven subunits the C-terminal hinge has moved closer to the closed conformation of loop-6, thereby avoiding the potential clash of the Leu178 side chain with the Trp170 side chain. In one subunit the C-terminal hinge has moved somewhat towards the bulk solvent, thereby also avoiding the clash with the Trp170 side chain; only in this subunit is the conformation of the N-terminal hinge residues Pro168-Val169-Trp170 the same as that in wild-type TIM. The tip of loop-6 is completely disordered in five subunits. In the three remaining subunits, three different paths for the main chain of loop-6 are observed. In two subunits the path is intermediate between the open and closed conformations, whereas in one subunit the path is completely different from the open or closed conformations, as shown in Fig. 5. In this conformation loop-6 has adopted a much more extended hairpin-loop-like conformation in which the Ile172-Gly173-Thr174-Gly175 peptide forms a turn at the tip of the hairpin. In this new conformation, the C^{α} atom of Ile172 has moved away from its standard closed and open positions by 7 and 8 Å, respectively. As shown in Fig. 6, this completely different conformation of loop-6 (in subunit *G*) is well defined by the corresponding electron-density map.

Interestingly, there are no apparent structural differences in the active sites of liganded wtTIM and liganded A178L (Fig. 7). This is in agreement with the structural studies of the liganded and unliganded YSL variant of chicken TIM, which showed that a leucine at position 178 is compatible with the wild-type closed conformation of loop-6. Also, the water structure in the active site is identical in the wtTIM and A178L liganded structures. In the atomic resolution structure of liganded wtTIM, four and two water molecules are hydrogen bonded to the phosphate moiety and the catalytic glutamate (Kursula & Wierenga, 2003), respectively, and these six waters are also observed in the liganded A178L structure (Fig. 7).

This study was initiated on the basis of the hypothesis that the A178L variant would stabilize a closed conformation of loop-6, generating a less active variant when introduced into wtTIM. The structural studies show that the C-terminal hinge indeed adopts a closed-like conformation, but loop-6 as a whole becomes partly disordered. The high degree of structural similarity between the liganded forms of wtTIM and A178L suggests that their small differences in kinetic properties are caused by the different properties of the unliganded

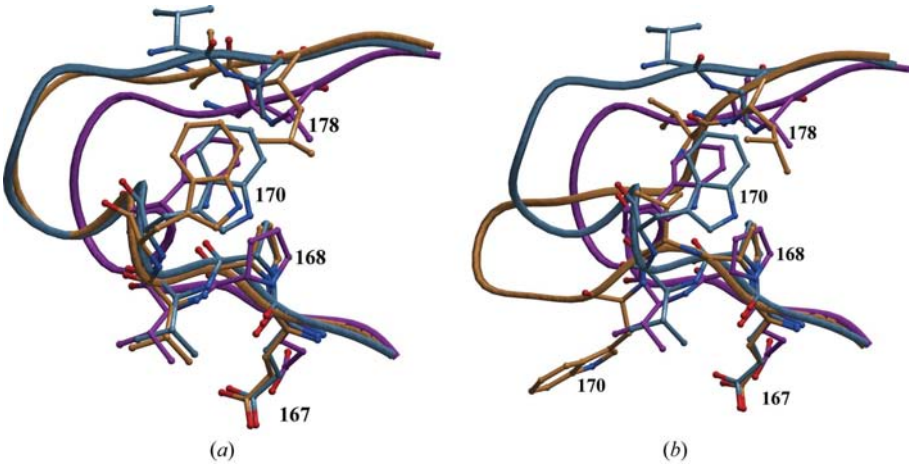

Figure 5
Schematic pictures (top view) of unliganded wtTIM (cyan) and liganded wtTIM (in magenta) together with loop-6 of a subunit of unliganded A178L. (*a*) Loop-6 of subunit *A* of unliganded A178L is also shown and is coloured gold. (*b*) Loop-6 of subunit *G* of unliganded A178L is included and is coloured gold. Note that in each case the Leu178 side chain of the mutant pushes the hinge of loop-6 towards the closed conformation.

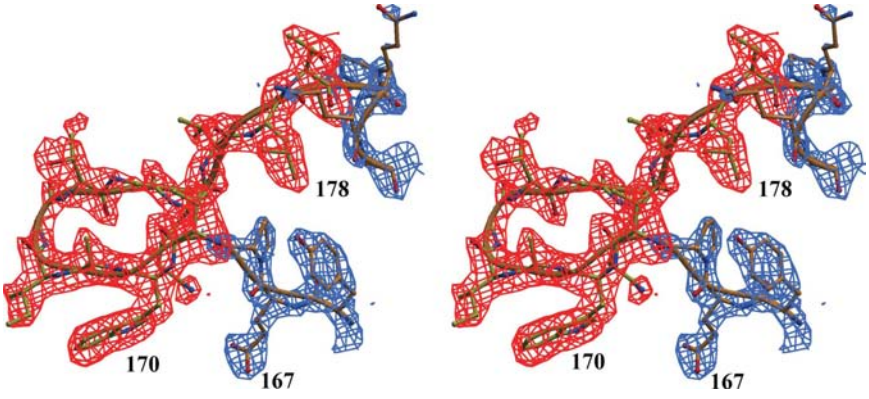

Figure 6
The electron-density map of loop-6 of subunit *G*. The maps were calculated from a refined OMIT model (in which residues 169–179 had been deleted) after OMIT refinement. The blue map (contoured at 2.0σ) is the $(2F_o - F_c)$, α_c map and the red map (contoured at 3.0σ) is the $(F_o - F_c)$, α_c map. Then same view is shown as in Fig. 5.

forms. Apparently, the more disordered loop-6 in unliganded A178L also shifts the equilibrium of 2PG binding in favour of the uncomplexed form, as the affinity of A178L for 2PG is lower than the wtTIM affinity for 2PG.

3.3. Structural studies of ml1A178L

The unliganded ml1A178L variant crystallized with one molecule per asymmetric unit. In the liganded ml1A178L crystal form there are three molecules per asymmetric unit (Table 1) and each of these adopted a very similar conformation. The refinement statistics are summarized in Table 2. Despite the marginal stability of ml1A178L (Fig. 4), diffracting crystals could be obtained of unliganded ml1A178L, providing a data set with a resolution of 2.3 Å but with a comparatively high Wilson *B* factor (Table 2). This structure has been refined with *REFMAC*5 (Murshudov *et al.*, 1997) to reasonable *R* factors and geometry (Table 2). In the structure of unliganded ml1A178L it is seen that the mutation induces a more closed conformation of the C-terminal hinge region, being the same as the conformation seen in subunit *B* of the unliganded A178L variant.

The crystals of unliganded ml1A178L were grown in the presence of 1.85 *M* phosphate. Nevertheless, no phosphate was bound at the phosphate binding site near loop-8 as seen in other TIM structures grown in the presence of sulfate or phosphate. Analysis of this

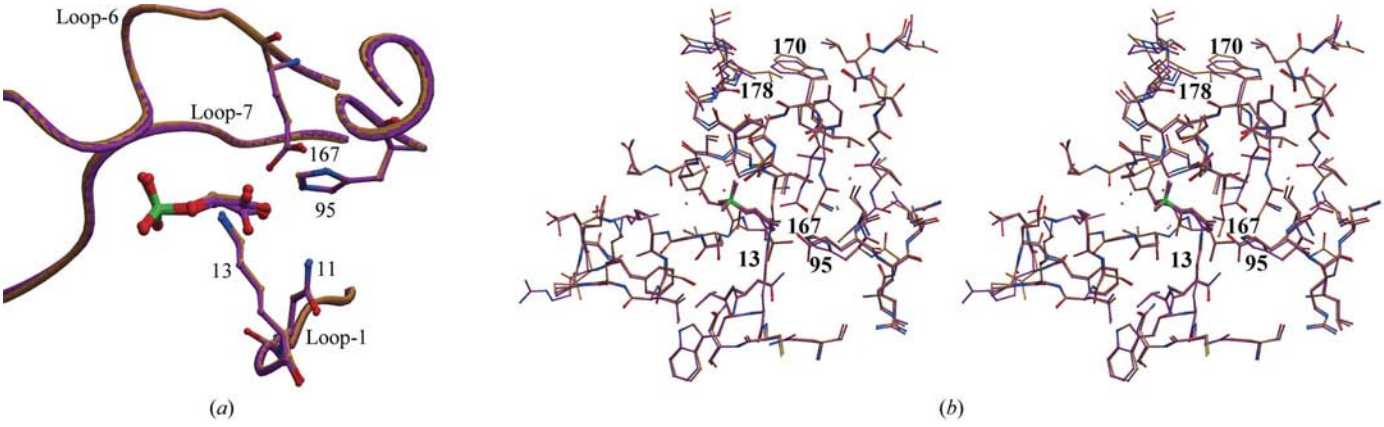

Figure 7
Comparison of the structures of liganded wtTIM (1n55; magenta) and liganded A178L (gold). (*a*) Schematic figure. (*b*) Stereoview. In wtTIM the ligand adopts two conformations. The mode of binding of 2PG to A178L corresponds to the major (up) conformation of the wtTIM complex. The water structure near the ligand and the catalytic glutamate is the same in both structures.

structure shows that the absence of phosphate binding is not a consequence of tight crystal contacts, but is instead a consequence of the switch of the peptide plane after Gly234 of loop-8. This small structural rearrangement, in which the main-chain region of loop-8 moves slightly towards the phosphate-binding pocket, is also apparent in Fig. 8. In this way, a favourable hydrogen bond to the phosphate (provided by Gly235 N) is lost and instead Gly234 O points into the wild-type phosphate-binding site, disfavouring binding. Such a peptide flip has never been observed in dimeric wtTIMs, but in at least one other unliganded monomeric TIM structure loop-8 also adopts a very different conformation (Borchert *et al.*, 1995; Norledge *et al.*, 2001), in which Gly234 O is flipped out.

The liganded ml1A178L crystal form diffracts to the near-atomic resolution of 1.18 Å and the structure has been refined with *SHELXL* (Sheldrick & Schneider, 1997). The crystal structure of liganded ml1A178L is essentially the same as previously observed for the structure of ml1TIM complexed with the transition-state analogue 2PG (Fig. 9; Thanki *et al.*, 1997). In the active site of this high-resolution liganded ml1A178L structure the phosphate moiety and the catalytic glutamate are seen to be hydrogen bonded to four and two water molecules, respectively, just as seen in the wtTIM complex (Fig. 7). These observations agree with the notion that the kinetic differences between ml1TIM and ml1A178L are correlated with the properties of its unliganded form, as was also noted for the A178L/wtTIM comparison. Like in wtTIM, the A178L mutation in ml1A178L does not induce a fully closed conformation of loop-6. However, the ml1A178L variant is much less stable and is already partly unfolded at the temperature of the assay. The lower k_{cat} values of ml1A178L can in part be explained from the partially unfolded state of this variant at the temperature of the assay (298 K).

For monomeric triosephosphate isomerases it has been noted that the loops that follow the β-strands have a larger structural plasticity than in wild-type TIM (Borchert *et al.*, 1995). The structural plasticity of ml1A178L is apparent from the peptide flip seen in loop-8 of the unliganded ml1A178L structure (Fig. 8) and from the large concerted shifts (more than 1 Å) of the helices following β-strands 1, 2, 3 and 4 when comparing unliganded and liganded ml1A178L (Fig. 8). These shifted regions are far away from the point-mutation site and also from the active site, suggesting that these structural changes are induced by different crystal contacts. In the wild-type TIM dimer these helices are at the dimer interface. Apparently, the monomer–monomer interactions in the wild-type dimer stabilize the positions of these helices with respect to the core of the subunit; such high structural plasticity of these helices is not observed in wild-type TIM. A larger structural plasticity has also been observed in some other monomeric variants of wild-

Figure 8
Comparison of the C$^{\alpha}$ traces of unliganded ml1A178L (gold) and ml1A178L complexed with 2PG (magenta). Note the small shifts of the helices (marked by a star) following β-strands 1, 2, 3 and 4. Also shown are the side chains of the four catalytic residues Asn11, Lys13, His95 and Glu167 as well as the side chain of Leu178. The label L8 identifies loop-8, in which a peptide flip has occurred in the unliganded structure.

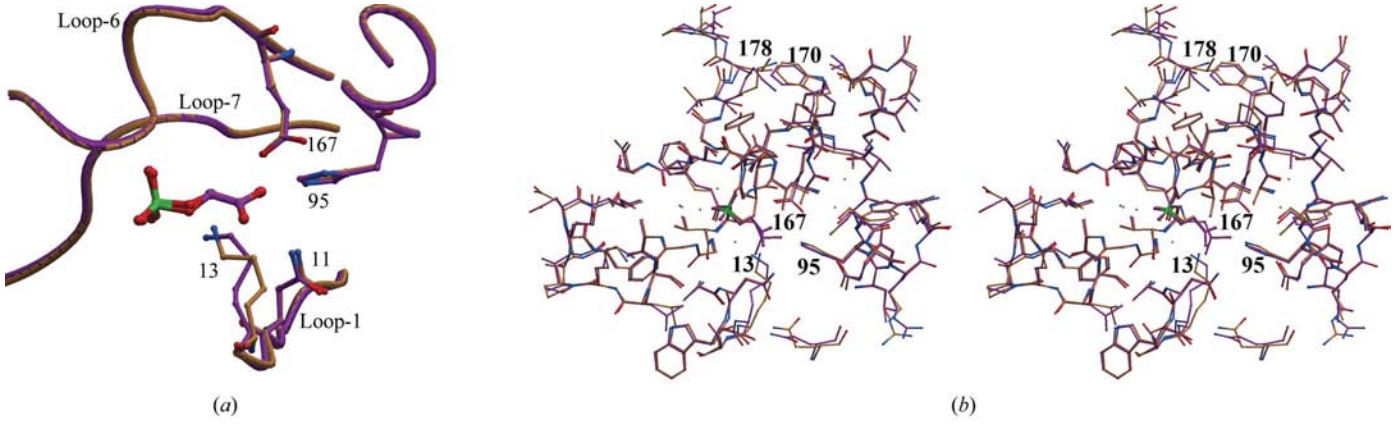

Figure 9
Comparison of the structures of liganded ml1TIM (1ml1) and liganded ml1A178L. (*a*) Schematic view. (*b*) Stereoview. The structure of ml1TIM is shown in magenta; ml1A178L is coloured gold.

type dimers, for example in the C-terminal domain of the HIV-1 virus capsid protein (Alcaraz *et al.*, 2007) and in chorismate mutase (Vamvaca *et al.*, 2004).

4. Concluding remarks

In wild-type TIM, a leucine is never observed at position 178 of the C-terminal hinge of loop-6 (Kursula *et al.*, 2004). Apparently, the natural selection process does not tolerate a leucine side chain at this position. The studies reported here provide possible explanations for this observation. For example, the different structural properties of loop-6 in the unliganded form of the A178L variant of wtTIM correlate with a twofold higher K_m value for both substrates, indicating that the variant has a lower affinity for its substrate, whereas the k_{cat} value is less affected (Table 3). TIM deficiency is known to cause severe diseases and evolutionary pressure has caused TIM to be a very efficient enzyme (Nickbarg & Knowles, 1988). It is possible that the lower affinity for substrate affects the catalytic efficiency *in vivo* to the extent that the changes in the intracellular metabolic flow induced by the A178L mutation are not tolerated. In addition, it is possible that the A178L mutation affects the *in vivo* folding and/or stability properties so much that this A178L variant does not function well enough in the cell.

Summarizing, in the liganded structure of A178L the active-site geometry and the conformations of loop-6 and loop-7 are very similar to those of the wild type. Also, the water structure near the bound 2-phosphoglycolate and near the catalytic glutamate is the same as in the liganded wild-type TIM structure. These studies have shown that the A178L point mutation particularly affects the properties of the unliganded form.

We thank the staff of beamlines BW7A and BW7B at DESY for skilful assistance. RKW is grateful to Dr Tsukihara for providing hospitality at the Institute for Protein Research at the University of Osaka, which very much facilitated the writing of this manuscript. We thank Ville Ratas for skilful technical assistance and Dr Koen Augustyns (University of Antwerp) for providing a sample of bromohydroxyacetone phosphate. This research was supported by grants from the Academy of Finland (project 53923). We thank the referees for their comments.

References

Alcaraz, L. A., Del Alamo, M., Barrera, F. N., Mateu, M. G. & Neira, J. L. (2007). *Biophys. J.* **93**, 1264–1276.
Amyes, T. L. & Richard, J. P. (2007). *Biochemistry*, **46**, 5841–5854.
Berlow, R. B., Igumenova, T. I. & Loria, J. P. (2007). *Biochemistry*, **46**, 6001–6010.
Borchert, T. V., Abagyan, R., Kishan, K. V., Zeelen, J. P. & Wierenga, R. K. (1993). *Structure*, **1**, 205–213.
Borchert, T. V., Kishan, K. V., Zeelen, J. P., Schliebs, W., Thanki, N., Abagyan, R., Jaenicke, R. & Wierenga, R. K. (1995). *Structure*, **3**, 669–679.
Casteleijn, M. G., Alahuhta, M., Groebel, K., El Sayed, I., Augustyns, K., Lambeir, A. M., Neubauer, P. & Wierenga, R. K. (2006). *Biochemistry*, **45**, 15483–15494.
Collaborative Computational Project, Number 4 (1994). *Acta Cryst.* D**50**, 760–763.
Desamero, R., Rozovsky, S., Zhadin, N., McDermott, A. & Callender, R. (2003). *Biochemistry*, **42**, 2941–2951.
Eaazhisai, K., Balaram, H., Balaram, P. & Murthy, M. R. (2004). *J. Mol. Biol.* **343**, 671–684.
Emsley, P. & Cowtan, K. (2004). *Acta Cryst.* D**60**, 2126–2132.
Gasteiger, E., Gattiker, A., Hoogland, C., Ivanyi, I., Appel, R. D. & Bairoch, A. (2003). *Nucleic Acids Res.* **31**, 3784–3788.
Gnerer, J. P., Kreber, R. A. & Ganetzky, B. (2006). *Proc. Natl Acad. Sci. USA*, **103**, 14987–14993.
Harris, T. K., Abeygunawardana, C. & Mildvan, A. S. (1997). *Biochemistry*, **36**, 14661–14675.
Jones, T. A., Zou, J.-Y., Cowan, S. W. & Kjeldgaard, M. (1991). *Acta Cryst.* A**47**, 110–119.
Joseph, D., Petsko, G. A. & Karplus, M. (1990). *Science*, **249**, 1425–1428.
Kabsch, W. (1993). *J. Appl. Cryst.* **26**, 795–800.
Kempf, J. G., Jung, J. Y., Ragain, C., Sampson, N. S. & Loria, J. P. (2007). *J. Mol. Biol.* **368**, 131–149.
Knowles, J. R. (1991). *Nature (London)*, **350**, 121–124.
Kursula, I., Salin, M., Sun, J., Norledge, B. V., Haapalainen, A. M., Sampson, N. S. & Wierenga, R. K. (2004). *Protein Eng. Des. Sel.* **17**, 375–382.
Kursula, I. & Wierenga, R. K. (2003). *J. Biol. Chem.* **278**, 9544–9551.
Kursula, P. (2004). *J. Appl. Cryst.* **37**, 347–348.
Lolis, E. & Petsko, G. A. (1990). *Biochemistry*, **29**, 6619–6625.
Lovell, S. C., Davis, I. W., Arendall, W. B. III, de Bakker, P. I., Word, J. M., Prisant, M. G., Richardson, J. S. & Richardson, D. C. (2003). *Proteins*, **50**, 437–450.
Massi, F., Wang, C. & Palmer, A. G. III (2006). *Biochemistry*, **45**, 10787–10794.
Murshudov, G. N., Vagin, A. A. & Dodson, E. J. (1997). *Acta Cryst.* D**53**, 240–255.
Nickbarg, E. B. & Knowles, J. R. (1988). *Biochemistry*, **27**, 5939–5947.
Noble, M. E., Zeelen, J. P. & Wierenga, R. K. (1993). *Proteins*, **16**, 311–326.
Norledge, B. V., Lambeir, A. M., Abagyan, R. A., Rottmann, A., Fernandez, A. M., Filimonov, V. V., Peter, M. G. & Wierenga, R. K. (2001). *Proteins*, **42**, 383–389.
Orosz, F., Olah, J. & Ovadi, J. (2006). *IUBMB Life*, **58**, 703–715.
Parthasarathy, S., Ravindra, G., Balaram, H., Balaram, P. & Murthy, M. R. (2002). *Biochemistry*, **41**, 13178–13188.
Pattanaik, P., Ravindra, G., Sengupta, C., Maithal, K., Balaram, P. & Balaram, H. (2003). *Eur. J. Biochem.* **270**, 745–756.
Pompliano, D. L., Peyman, A. & Knowles, J. R. (1990). *Biochemistry*, **29**, 3186–3194.
Ralser, M., Heeren, G., Breitenbach, M., Lehrach, H. & Krobitsch, S. (2006). *PLoS ONE*, **1**, e30.
Rozovsky, S., Jogl, G., Tong, L. & McDermott, A. E. (2001). *J. Mol. Biol.* **310**, 271–280.
Rozovsky, S. & McDermott, A. E. (2001). *J. Mol. Biol.* **310**, 259–270.
Sampson, N. S. & Knowles, J. R. (1992*a*). *Biochemistry*, **31**, 8482–8487.
Sampson, N. S. & Knowles, J. R. (1992*b*). *Biochemistry*, **31**, 8488–8494.
Schliebs, W., Thanki, N., Eritja, R. & Wierenga, R. K. (1996). *Protein Sci.* **5**, 229–239.
Sheldrick, G. M. & Schneider, T. R. (1997). *Methods Enzymol.* **277**, 319–343.
Sun, J. & Sampson, N. S. (1999). *Biochemistry*, **38**, 11474–11481.
Thanki, N., Zeelen, J. P., Mathieu, M., Jaenicke, R., Abagyan, R. A., Wierenga, R. K. & Schliebs, W. (1997). *Protein Eng.* **10**, 159–167.
Vagin, A. & Teplyakov, A. (1997). *J. Appl. Cryst.* **30**, 1022–1025.
Vamvaca, K., Vogeli, B., Kast, P., Pervushin, K. & Hilvert, D. (2004). *Proc. Natl Acad. Sci. USA*, **101**, 12860–12864.

Wierenga, R. K., Noble, M. E., Postma, J. P., Groendijk, H., Kalk, K. H., Hol, W. G. & Opperdoes, F. R. (1991). *Proteins*, **10**, 33–49.
Wierenga, R. K., Noble, M. E., Vriend, G., Nauche, S. & Hol, W. G. (1991). *J. Mol. Biol.* **220**, 995–1015.
Williams, J. C. & McDermott, A. E. (1995). *Biochemistry*, **34**, 8309–8319.
Williams, J. C., Zeelen, J. P., Neubauer, G., Vriend, G., Backmann, J., Michels, P. A., Lambeir, A. M. & Wierenga, R. K. (1999). *Protein Eng.* **12**, 243–250.
Xiang, J., Jung, J. Y. & Sampson, N. S. (2004). *Biochemistry*, **43**, 11436–11445.
Zeelen, J. P., Hiltunen, J. K., Ceska, T. A. & Wierenga, R. K. (1994). *Acta Cryst.* D**50**, 443–447.